AEROTHERMODYNAMIC OPTIMIZATION AND DESIGN ANALYSIS OF A NOVEL REUSABLE LAUNCH VEHICLE USING NUMERICAL TECHNIQUES

Fariha Rahman[1]
Incoming Postgraduate Student, Institute of Aerospace Science, University of Toronto, Canada
Srinivas G[2*]
Associate Professor, Department of Aeronautical & Automobile Engineering, Manipal Institute of Technology (MIT), Manipal Academy of Higher Education (MAHE), Manipal, Karnataka, India – 576104
Md Shakil Hossen Gibon[3]
Graduate Student, Aeronautical Engineering, National University, Bangladesh

ABSTRACT

The design and analysis of a new reusable launch vehicle (RLV) inspired by the HTV and Lockheed Martin X-33 are presented in the study, featuring unique modifications in both the nose and rear sections to generate a strong shockwave and minimize body heating. The primary focus of this study is to conduct a numerical analysis to predict enhancements in the aerothermodynamic parameters of the RLV under hypersonic conditions during re-entry. The investigation was conducted in three stages: (i) Grid Sensitivity Test, (ii) Turbulence Model Validation, and (iii) Aerodynamic Heating Analysis across Mach numbers ranging from 5 to 12. The grid sensitivity analysis identified 0.31 million elements as optimal, with the K-ω SST turbulence model demonstrating superior accuracy in predicting pressure coefficients and thermal behavior. Comparative assessments revealed the K-ω SST model as the most effective for near-wall viscosity and heat transfer reduction, while the blunt nose design significantly mitigated peak temperatures by creating a detached shock wave. Lastly, the aerodynamic heating characteristics of a newly designed Reusable Launch Vehicle (RLV) were evaluated under hypersonic conditions using the K-ω SST turbulence model, focusing on Mach numbers ranging from 5 to 12. The heat transfer coefficients at stagnation points, calculated using the Fay-Riddel equation, were compared with CFD results across Mach numbers 5 to 12, revealing that Mach 10.5 showed the highest accuracy with a 25.9% discrepancy, while discrepancies were more pronounced at Mach numbers 8 and 12. By this study it was found that the thermal management was improved, higher lift-to-drag ratios were achieved, and peak heat transfer was reduced by the blunt nose design and optimized configurations, thereby enhancing the vehicle's structural integrity and mission success during re-entry. Thus, the innovative RLV design has the potential to revolutionize the future of reusable launch vehicles, offering cost-effective, long-term service for the aerospace industry. Significant

[2*] Corresponding author email: srinivas.g@manipal.edu

financial and functional advantages could arise from its industrialization by NASA or other aerospace producers in the future.

NOMENCLATURE, ACRONYMS, ABBREVIATIONS

C_l	lift coefficient
C_d	drag coefficient
C_m	moment coefficient
C_p	pressure coefficient
L/D	lift-to-drag ratio
ρ	density
ν	velocity
l_{ref}	reference length
S_{ref}	reference surface area
L	lift
D	drag
P	pressure
T	temperature
R	gas constant
k	thermal conductivity
μ	first coefficient of viscosity
λ	second coefficient of viscosity
∇^2	Laplacian operator
h	stagnation point heat transfer coefficient
ρ	density
μ	viscosity
$(\frac{dU}{dx})_{x=0}$	velocity gradient at the stagnation point
R_{eff}	nose radius of the reentry vehicle

AUSMD	advection upstream splitting method
AOA	angle of attack
SST	shear stress transport
RLV	reusable launch vehicle
CFD	computational fluid dynamics
LES	large eddy simulation
TPS	thermal protection system
TPSOPT	thermal protection system optimization of hypersonic vehicle
RANS	Reynolds-averaged Navier–Stokes
ASA	Advanced Structural Assembly
MDO	multidisciplinary design optimization
NASA	National Aeronautics and Space Administration
ATAC	Aeroheating and Thermal Analysis Code
HTV	Hypersonic Technology Vehicle

Subscripts:

∞	free stream
w	wall
s	stagnation
ref	reference

INTRODUCTION

The design and development of reusable launch vehicles have been a major focus in the aerospace industry, driven by the need for cost-effective and sustainable access to space. As the industry aims to lower the cost of space travel and reduce the environmental impact of space missions, reusable launch vehicles (RLVs) have emerged as a promising solution. One critical aspect of this endeavor is the optimization of the vehicle's aerodynamic and aerothermodynamic characteristics, which can significantly impact its performance, efficiency, and safety during the launch and re-entry phases. Optimizing these characteristics is a complex and multi-faceted challenge that involves understanding and controlling the interactions between the vehicle and the atmospheric environment it traverses. During launch, the vehicle must efficiently penetrate the dense lower atmosphere, minimizing drag and fuel consumption. Upon re-entry, it must withstand extreme thermal loads and aerodynamic forces while maintaining structural integrity and controllability. Achieving a balance between these competing demands requires sophisticated design and analysis techniques.

In this research paper, our study encompasses various aspects of the vehicle's design, including proposing a new model, and analyzing its aerodynamics and aerothermal aspects while reentry using advanced numerical techniques, providing a holistic approach to the development of next-generation RLVs. By leveraging state-of-the-art computational fluid dynamics (CFD) simulations and optimization algorithms, it was aimed to develop a vehicle design that maximizes performance and safety while minimizing operational costs.

Several researchers have focused on various aspects of this optimization to improve the performance, efficiency, and safety of these vehicles during launch and re-entry phases. Their work involved comparing laminar and turbulent predictions with wind tunnel and flight condition data, achieving close agreement and providing greater confidence in the aerodynamic and aero-heating database for the vehicle[1]**.** P.C. Chen et al. developed an automated 3D design procedure called TPSOPT, which aims to minimize the thermal protection system (TPS) weight while satisfying structural constraints and thermal protection requirements. The methodology was demonstrated using a modeled X-34, optimizing the TPS thickness distribution through assigned shape functions combined with a complex variable differentiator and the optimizer ASTROS[2]. Similarly, Devashish Bhalla et al. conducted numerical simulations to study the aerothermal characteristics of a typical re-entry/crew module in hypersonic flow regimes. They utilized the CFD++ software with a RANS solver to analyze various aerodynamic parameters and stagnation point heat flux variations across different Mach numbers[3].

The validation of heat flux with flight data was also performed using an in-house developed code for crew module atmospheric re-entry experiments, demonstrating the importance of accurate heat flux predictions in RLV design [4]. Francesco Battista et al. presented a simplified methodology to evaluate the time history of the aerothermal environment over a wing as part of the Advanced Structural Assembly (ASA) project funded by the Italian Space Agency and Thales Alenia Space. This methodology aimed to provide reliable results within a reasonable time frame, contributing to the development of reusable experimental re-entry vehicle wings[5]. Besides, Simone Di Giorgio and colleagues developed a highly integrated design environment for aerothermodynamic optimization. This environment included modules for geometrical parameterization, automated

data transfer between tools, computational analysis codes, and design optimization methods, facilitating an efficient and streamlined optimization process[6].

Again, Sheffer and Dulikravich assessed the constrained optimization of three-dimensional aeroshapes, focusing on reducing aerodynamic drag while considering vehicle volume and length constraints[7]. Additionally, Bowcutt developed a multidisciplinary design optimization (MDO) approach that combines propulsion, external aerodynamic forces, mass properties, and internal volumetric modeling to maximize the mission range of a hypersonic cruise missile[8]. Further, Lobbia conducted an MDO of the NASA HL-20 concept, with the goal of maximizing aerodynamic efficiency while considering re-entry heating as a constraint[9].

Moreover, McNamara et al. expanded the understanding of hypersonic aerothermoelasticity by investigating fluid-thermal-structural coupling and developing frameworks to reduce the computational effort associated with aerothermoelastic analysis[10]. Kuzenov and Ryzhkov formulated an approximate mathematical model for calculating heat transfer processes and resistance coefficients for high-speed aircraft, including the X-33 and X-43 vehicles[11]. Pezzella and Viviani analyzed the aerodynamic performance of a winged re-entry vehicle, emphasizing its high lift capabilities from low Earth orbit[12]. Musharraf et al. investigated the use of aerospike structures to mitigate aerodynamic drag in hypersonic vehicles, demonstrating significant drag reduction through numerical simulations that were validated by experiments[13].

Furthermore, Kumar and colleagues focused on shape optimization for re-entry vehicles, exploring configurations with sharp and blunt spikes to minimize re-entry heating and aerodynamic drag[14]. Murray utilized the Aeroheating and Thermal Analysis Code (ATAC) for planetary re-entry environments, integrating it with other codes to generate finite element thermal boundary conditions for missile design[15]. G. Gopala Krishnan, Akhil, and Nagaraja S R successfully conducted a Numerical study on the design of re-entry vehicles, focusing on the balance between reducing aerodynamic drag and managing heat dissipation by using single-spike and twin-spike configurations on blunt bodies[16]. Another research titled "Aerodynamic Design Exploration for Reusable Launch Vehicle Using Genetic Algorithm with Navier Stokes Solver" was conducted by Tomoaki Tatsukawa, Taku Nonomura, et al. that aimed to understand aerodynamic behaviors and gain design insights for various shape configurations using a genetic algorithm combined with a Navier-Stokes solver[17]. These studies collectively contribute to the body of knowledge necessary for optimizing the aerodynamic and aerothermodynamic characteristics of reusable launch vehicles, advancing the field toward more efficient and reliable space transportation systems.

In this research, inspired by Martin X-33 and HTV, an innovative reusable launched vehicle (RLV) was modeled, that will be able to present several aerodynamic advantages derived from its innovative features. The incorporation of a blunt nose design would allow for the generation of a robust shockwave, which would effectively increase the heating of the surrounding air while minimizing heat transfer to the vehicle body [18].This characteristic would be crucial for contributing to the objective of reducing vehicle body heating during re-entry, enhancing the overall safety and durability of the RLV. On top of that, the upward-curved wings that are fully integrated with the vehicle body, along with the two body flaps located at the rear, enhance maneuverability and control. In this case, the vehicle will have more drag than the lift, which will

slow the body down during its re-entry. The vertical stabilizer positioned at the top rear edge provides effective yaw control, while the body flaps, in conjunction with the curved wings, facilitate improved pitch and roll control. This configuration would not only be optimized for aerodynamic performance during various flight phases but also have its stability and responsiveness enhanced, making it better suited for complex flight maneuvers. Overall, the vehicle's efficiency, control, and thermal management during re-entry and other flight operations would be collectively improved by these aerodynamic features. To accurately predict the aerothermal behaviors of the novel vehicle the whole study was conducted using different tests including grid sensitivity check for varying numbers of grid elements, turbulence model validation check deferring four turbulence models namely-K-ω SST, K-ε Realizable, K-ε Standard, LES, etc. Lastly, another study was performed by changing the boundary conditions several times for a range of Mach numbers i.e. 5, 6, 8, 8,82, 10, 10.5, 12, etc. to get better aerothermal results for Cp, total temperature, and heat flux for the unique model at re-entry conditions. Our future research will be focused on the improvement of the stability and aerodynamic control system of this new re-entry vehicle. The innovative design of this reusable launch vehicle (RLV) holds significant potential for future contributions to the aerospace industry, including organizations like NASA and SpaceX, by offering enhanced aerodynamic efficiency, control, and thermal management. Its advanced features could certainly lead to more cost-effective, safe, and sustainable access to space, paving the way for more frequent and reliable missions.

METHODOLOGY

In this paper, the aerothermal parameters of the RLV model have been tested using some conventional numerical approaches. The below-mentioned methods are crucial enough to predict the aerothermal behaviors i.e. Cp, total temperature, heat flux, Mach numbers, etc.

3D RLV modeling

The model is developed using SolidWorks 2020, and exhibits similar length and height dimensions with the HTV×Martin X-33 but includes several structural modifications for targeted better aerodynamic and thermal performance during atmospheric re-entry [1]. The model has been scaled down to a 10:1 ratio, yielding an overall length of 315.5 mm. The wing span measures 278.22 mm, with the wings angled at 21.81° relative to the horizontal body.

The tail has been redesigned to a height of 33.5 mm and a length of 47 mm. The fuselage height is 37.1 mm, featuring modifications in the rear section. The winglets, each 25.7 mm in height, are oriented approximately 90° to the wings. The nose is blunted at an angle of 56.04° to reduce bow shock and intense heating during re-entry. The body flap, with dimensions of 31.35 mm in width and 37.55 mm in length, is set at an angle of 9.91° to enhance lift generation. The visual representation of the 3D re-entry vehicle has been presented on the Figure 1. These modifications collectively optimize the model's aerodynamic and thermal management characteristics.

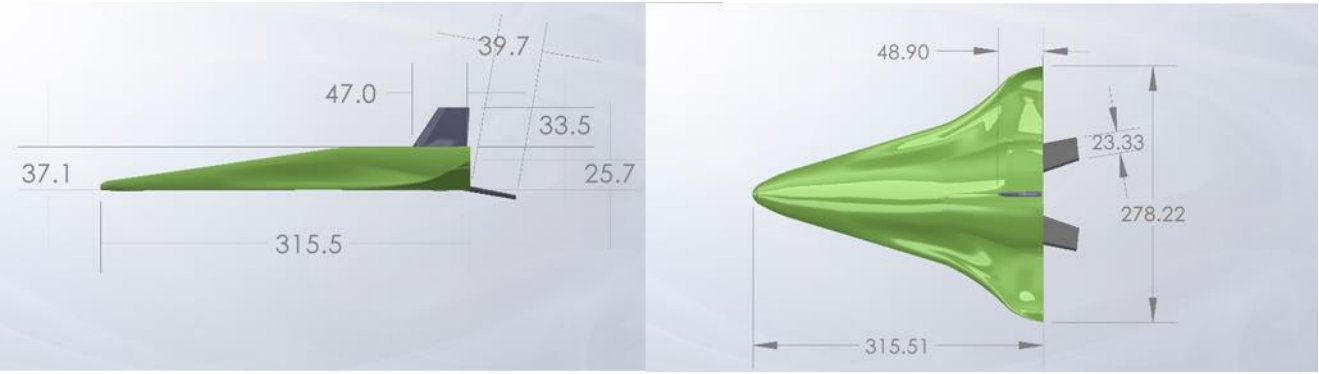

(b) Side View of 3D RLV (a) Top View of 3D RLV

Figure 1. 3D RLV Geometry showing (a) Side View and (b)Top View [1]

Meshing

The SOLIDWORKS model of the Reusable Launch Vehicle was imported into ANSYS Fluent 19.2 for mesh generation. A rectangular far-field enclosure, with dimensions of 98 inches in length and 70 inches in both height and width, was utilized, representing nearly 5 to 7 times the RLV model's width and height, respectively. To comply with the $y \leq 1$ criterion for effective boundary-layer resolution across various Mach numbers, the initial grid spacing perpendicular to the wall was set at 90 mm using a tetrahedron mesh type[19]. The mesh details are given on the Table 1. Following this, the inlet, outlet, and enclosure walls were appropriately selected, and the ANSYS 19.2 tool was used to construct an unstructured mesh for the RLV, consisting of 671,492 mesh elements [20]. Lastly, to ensure the targeted resolution in critical areas of the simulation domain, the mesh was systematically refined through the application of face sizing and inflation techniques. This approach was implemented to achieve near-wall grid refinement, which is essential for accurately capturing viscous effects. The first layer thickness was determined based on the criterion of $Y+ = 1$, allowing for improved representation of the boundary layer. To achieve a more refined mesh Face sizing was utilized. Detailed specifications of the RLV vehicle mesh are provided in Table II, while Fig. 2 illustrates both the high-resolution full grid view and the close-up grid view, highlighting the mesh quality and resolution achieved in the analysis.

Table 1. Mesh Details

Names	Description
Grid size	90mm
Face sizing	80 mm
Inflation	first layer
Elements	671492
Nodes	195040

Mesh method	Tetrahedron
Orthogonal quality	0.051
First layer thickness	2.26E-05
Reynold number	7.89E+06
Kinematic viscosity m^4/s	8.012E-04
Y+	1

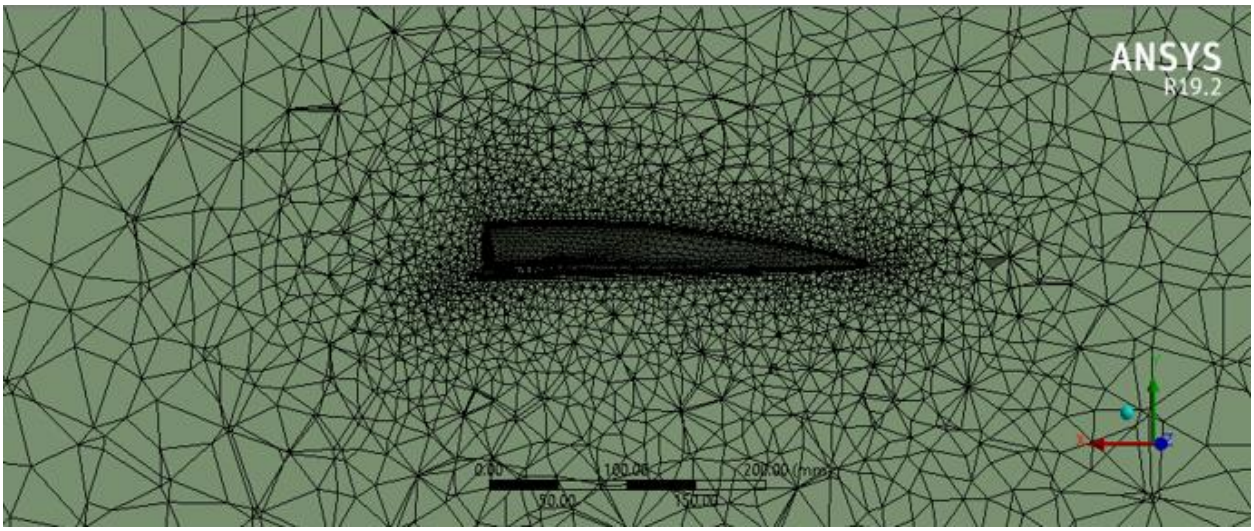

Figure 2. Close Grid View of Mesh

Numerical Analysis Procedures

In this study, numerical analysis was performed using ANSYS Fluent version 19.2. The investigation focused on the hypersonic compressible flow around the RLV, utilizing a density-based, steady-state solver while incorporating the energy equation. To enhance the simulations of the hypersonic re-entry vehicle, the K-ω SST turbulence model was employed with the second-order upwind implicit AUSMD scheme, ensuring robustness in handling complex geometries and accurately predicting wall-bounded flows, including boundary layers, while improving convergence accuracy and computational stability. The k–ω SST model is generally used for hypersonic flow analysis due to its accurate near-wall modeling, which captures complex interactions between the hypersonic flow and the vehicle's surface [21]. It effectively handles adverse pressure gradients and reduces sensitivity to free stream conditions, improving stability and accuracy in hypersonic simulations [22]. By combining the strengths of the k–ω model for boundary layers and the k-ε model for outer flow, the SST model provides a comprehensive approach to turbulence capture across the full spectrum of the boundary layer and external flow [23].It is the most frequently utilized model in the industry due to its excellent balance between

accuracy and cost-effectiveness. In addition, various turbulence models, including K-ε Realizable, K-ε Standard, and LES, were employed to validate the turbulence model in relation to the vehicle design for CFD simulation. For the boundary conditions, a velocity inlet was selected for the inlet and a pressure outlet for the outlet to simulate the free stream Mach numbers and static parameters resulting from the aerodynamic simulations.

Furthermore, to achieve more precise predictions, multiple CFD analyses were conducted across various scenarios, including changes in Mach numbers from 6 to 12 and different boundary conditions, which are detailed in the subsequent sections. The boundary layer flow was accurately represented by employing a well-suited combination of turbulence models and near-wall grid resolution, with an initial grid spacing of 90 mm. An overview of the CFD solution process is summarized in Table 2. The simulations were calculated using Intel[R] Core [TM] i5-104000 CPU 2.90 GHz, a total of 6 logical processors and it took 10-15s CPU time per iteration. Achieving convergence in hypersonic CFD analysis is challenging due to the transient nature of the flows, intense shock waves, and complex turbulence. The need for more iterations is driven by particular flow characteristics, numerical methods, and the computational demands of high-resolution meshes. Consequently, 5,000 iterations were performed to handle the fine mesh resolution and accurately manage the hypersonic flow conditions.

Table 2. Details of Numerical Analysis

Names	**Description**
Solver	Steady-state, density based, energy equation
Air density	Ideal Gas
Air viscosity	Sutherland three coefficients
Turbulence model	K–ω SST
Scheme	AUSMD implicit
Courant	0.35
Convergence criteria	10^-05
Iterations	5000

Theoretical Calculation of Aerodynamic Heating

To predict the appropriate aerothermal effects of the RLV, coefficients of stagnation points were measured for different Mach cases using specific equations. Upon completion of the theoretical calculations, the results were compared with CFD outcomes to validate the model and its aerodynamic heating conditions at high speed. The stagnation point heat transfer coefficient was analyzed to facilitate re-entry trajectory planning and ensure that the vehicle can withstand the thermal environment encountered—stagnation point Heat transfer coefficient [24]. A broad

explanation has been given on the below section. The entire process of this experiment has been depicted in Figure 3.

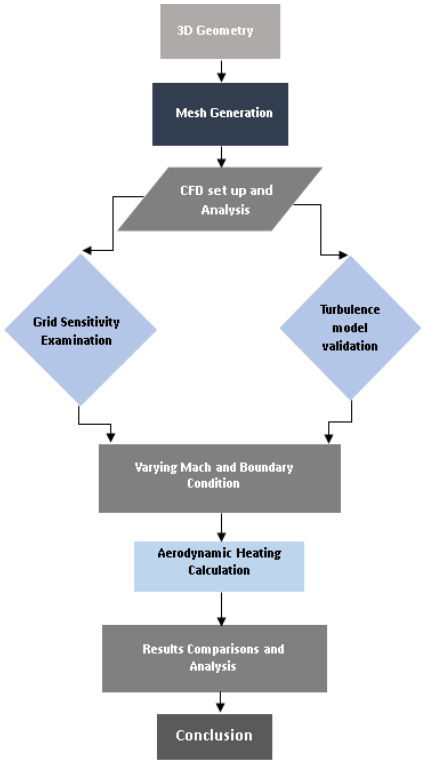

Figure 3. Work Flow

NUMERICAL EQUATION

In this study, the numerical analysis for predicting the aerodynamics of a hypersonic RLV vehicle was conducted using the Navier-Stokes equations in conjunction with the K-ω SST turbulence model [17]. The Navier-Stokes equations, which describe the most general single-phase fluid flow, were employed. Specifically, the equations used in the CFD analysis were formulated in Cartesian coordinates as presented in equations [22] (1)-(6).

Continuity equation

$$\frac{\partial \rho}{\partial t} + \frac{\partial (\rho u)}{\partial x} + \frac{\partial (\rho v)}{\partial y} + \frac{\partial (\rho w)}{\partial z} = 0 \tag{1}$$

x momentum equation

$$\rho \frac{\partial u}{\partial t} + \rho u \frac{\partial (u)}{\partial x} + \rho v \frac{\partial (u)}{\partial y} + \rho w \frac{\partial (u)}{\partial z} = -\frac{\partial p}{\partial x} \tag{2}$$

y momentum equation

$$\rho\frac{\partial v}{\partial t}+\rho u\frac{\partial(v)}{\partial x}+\rho v\frac{\partial(v)}{\partial y}+\rho w\frac{\partial(v)}{\partial z}=-\frac{\partial p}{\partial y} \tag{3}$$

z momentum equation

$$\rho\frac{\partial w}{\partial t}+\rho u\frac{\partial(w)}{\partial x}+\rho v\frac{\partial(w)}{\partial y}+\rho w\frac{\partial(w)}{\partial z}=-\frac{\partial p}{\partial z} \tag{4}$$

Energy

$$\frac{\partial s}{\partial t}+u\frac{\partial(s)}{\partial x}+v\frac{\partial(s)}{\partial y}+w\frac{\partial(s)}{\partial z}=0 \tag{5}$$

For a calorically perfect gas can be replaced by the following equation-

$$\frac{\partial}{\partial t}\left(\frac{p}{\rho^{\gamma}}\right)+u\frac{\partial}{\partial x}\left(\frac{p}{\rho^{\gamma}}\right)+v\frac{\partial}{\partial y}\left(\frac{p}{\rho^{\gamma}}\right)+w\frac{\partial}{\partial z}\left(\frac{p}{\rho^{\gamma}}\right)=0 \tag{6}$$

Where u, v, w denotes fluid velocity vectors, P is pressure, ρ is density, μ is kinematic viscosity and ∇^2 is a Laplacian operator.

Additionally, for the viscous compressible flow of ideal gas Navier Stoke's governing equations are expressed as follows [25]

$$\rho\left[\frac{\partial V}{\partial t}+(V.\nabla)V\right]=-\nabla P+\nabla.[\lambda(\nabla.V)\bar{I}]+\nabla.[\mu(\nabla V+\nabla V^{tr})] \tag{7}$$

$$\frac{\partial\rho}{\partial t}+\nabla.(\rho V)=0 \tag{8}$$

$$\rho C_p\left[\frac{\partial T}{\partial t}+(V.\nabla)T\right]=\nabla.(k\nabla_T)+\frac{\partial\rho}{\partial t}+(V.\nabla)P+\Phi \tag{9}$$

$$P=\rho RT \tag{10}$$

Where, V is the velocity vector, ρ is density, P denotes pressure, T is temperature, R is the gas constant, k denotes thermal conductivity, μ and λ are the first and second coefficients of viscosity respectively. However, the viscous dissipation Φ can be written as

$$\Phi=\lambda(\nabla.V)^2+\frac{\mu}{2}(\nabla V+\nabla V^{tr})^2 \tag{11}$$

Again, the aerodynamic analysis is established based on lift (C_l), drag (C_d) and pitching moment (C_m) which are computed as stated by the following equations:

$$C_l = \frac{L}{0.5\,\rho v^2\, S_{ref}} \tag{12}$$

$$C_d = \frac{D}{0.5\,\rho v^2\, S_{ref}} \tag{13}$$

$$C_m = \frac{M}{0.5\,\rho v^2\, l_{ref} S_{ref}} \tag{14}$$

Where, L, D, and M represent lift, drag, and Moment respectively, ρ is density, v is velocity, S_{ref} and l_{ref} imply the surface area of the wing and length respectively.

THEORETICAL EQUATION FOR AERODYNAMIC HEATING CALCULATION

Calculating the Fay-Riddell equations is crucial for understanding aerodynamic heating at the stagnation point during hypersonic re-entry. The Fay-Riddell equation provides a method to estimate the heat transfer rate at the stagnation point of a reentry vehicle moving at hypersonic speeds. The Fay-Riddell equation is often used to validate modern computational fluid dynamics (CFD) solutions. Its accuracy in predicting heat flux makes it a reliable benchmark. The modified versions of the equations given by Fay and Riddell [26] are stated as-

$$h = 0.94 K_1 (\rho_s \mu_s)^{0.4} (\rho_w \mu_w)^{0.1} \sqrt{\left(\frac{dU}{dx}\right)_{x=0}} \tag{15}$$

where velocity gradient states as:

$$\left(\frac{du_e}{dx}\right)_s = \frac{1}{R_{eff}} \sqrt{\frac{2(p_s - p_\infty)}{\rho_s}} \tag{16}$$

$K_1 = 1$ for the axisymmetric body, ρ_s is static density, ρ_w is wall density, μ_s is the viscosity at the static condition and μ_w is the viscosity of the wall.

RESULTS AND DISCUSSION

Grid Sensitivity Check

Grid sensitivity analysis is crucial for ensuring the accuracy and reliability of numerical results in hypersonic reentry simulations, capturing complex flow phenomena such as shock waves and high-temperature effects. It optimizes grid resolution to balance accuracy and computational cost, validating CFD models against experimental or theoretical data [19]. The first stage of this research

was to conduct the grid independence study to achieve the best grid size along with grid quantity that can be further used to accurately predict the overall and near-wall aerodynamic flow behaviors of the designed RLV. Considering, the Y+ in the near-wall as 1, with an initial spacing of 0.09m the baseline test was conducted to predict the best grid quantity that would provide the best aerodynamic features through simulations. Here, k-ω SST was utilized along with mach 6. This resulted in having the number of grid elements 320738 following a pressure coefficient, Cp of 0.98.

Afterward, the analysis was continued for several other grid sizes i.e. 95mm, 85mm, 80mm, 75mm, and 70mm. The number of grid elements obtained from this test were presented on the Table 3 which shows that for grid sizes 70, 80, and 85 a similar quantity of grid elements was obtained which was about 0.31M. Similarly, for grid sizes 75mm and 95mm the largest number of elements were found which is around 0.42M. The grid elements obtained from different grid sizes have been tabulated on Table 3.

Table 3. Grid Quantity for Different Grid Sizes

Edge Sizing Element Size mm	**Face Sizing 2 Element Size** mm	**Mesh Elements**
65	65	314270
70	70	421512
75	75	314270
75	75	314270
80	80	320738
85	85	421512

The variations of results for pressure coefficients, C_p obtained for different grid quantities are shown in the Figure 4. By analyzing the flow contours presented in Figure 5 it can be said that for element number 0.32 M the highest C_p was predicted that be 0.98 whereas C_p 0.76 was found for element number 0.42 M. However, for the grid quantity 0.31M, the pressure coefficient was obtained as 0.45 that has a better correlation with the reference data[27]. Table 4 presents the validation of the grid sensitivity test by comparing the reference paper data with the CFD results for C_p. It can be seen that for the grid elements, 0.31 million there was the least error of approximately 6% compared with the other grid quantities 0.32M and 0.42 M which have errors of nearly -31% and -46.9% respectively. The lift coefficient was observed to be negative, attributed to the fixed angle of attack (AOA) set at 0 degrees. It is noted that most re-entry vehicles re-enter the atmosphere with an AOA between 10 and 25 degrees. Future research will focus on exploring

the effects of varying AOA on control and stability. A good correlation between obtained Cp and the reference Cp flow contours can be seen on Figure 6.

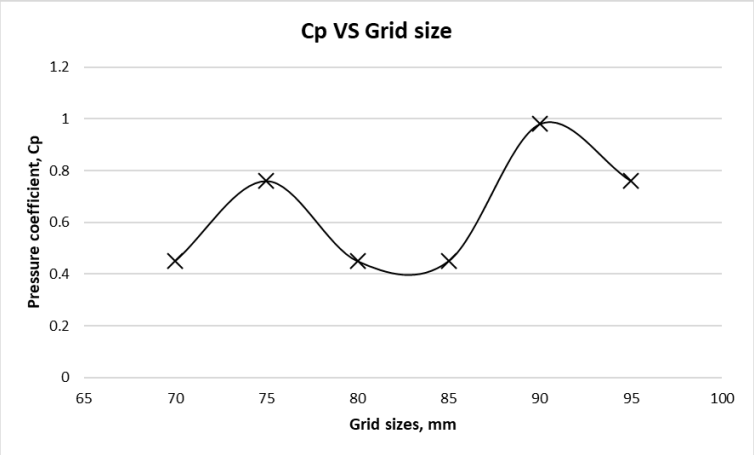

Figure 4. Variation in Pressure Coefficients with changing Grid Sizes

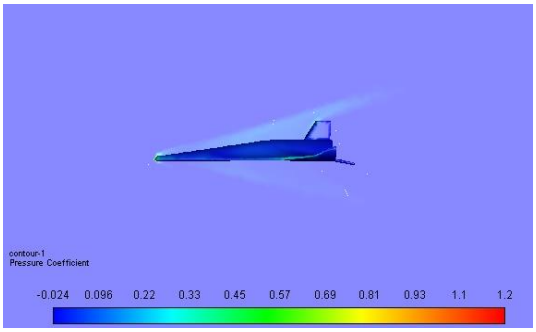

(a)Element number 0.31M

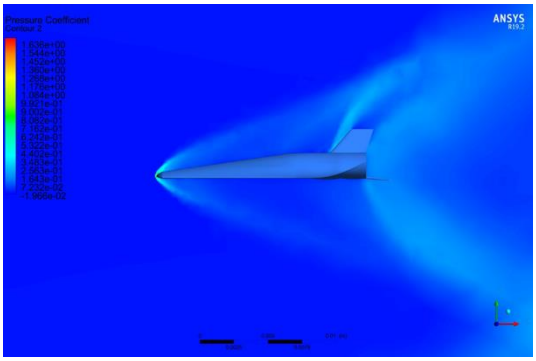

(b)Element number 0.32M

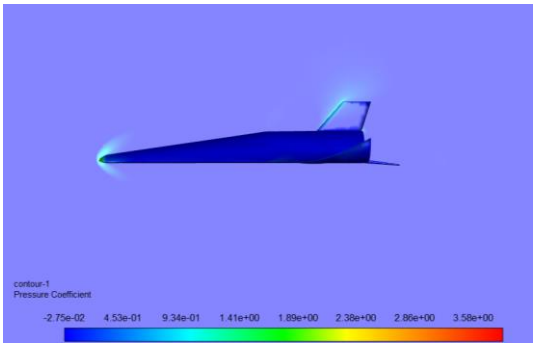

(c)Elements 0.42M

Figure 5. Pressure Coefficient flow contours for (a) Element number 0.31M, (b) Element number 0.32M, and (c) Element number 0.42M

Table 4. Comparisons between obtained CFD data and Reference data for Cp [27]

Obtained data		Ref Data	
Mesh Elements	**Cp**	**Cp**	**Error%**
0.31 M	0.49	0.52	6.122449
0.42 M	0.76	0.52	-31.5789
0.32 M	0.98	0.52	-46.9388

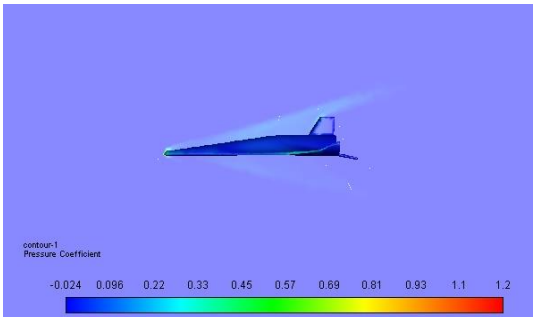

(a) Element number 0.31M

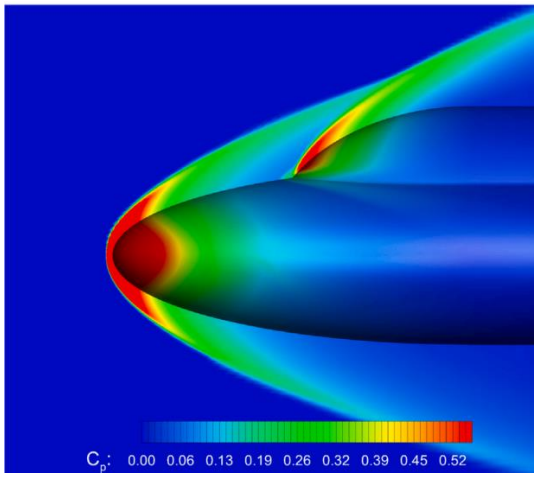

(b) Ref Flow contour of Pressure coefficient

Figure 6. Flow contours showing a comparison between Cp obtained from Grid element 0.31M and Reference Cp [27]

Turbulence Model Validation Check

During hypersonic re-entry, the surface roughness of a vehicle significantly influences its aerodynamic coefficients by increasing both heat flux and skin friction. This necessitates the use of Computational Fluid Dynamics (CFD) analysis to accurately assess these impacts. To predict turbulence with high fidelity, numerical investigations were conducted in this experiment utilizing four turbulence models: K-ε realizable, K-ω SST, K-ε standard, and LES. The K-ε realizable model is well-suited for computing flow behaviors away from boundaries, while the K-ω SST model excels in simulating flow within viscous sublayers[28].

Initially, the K-ω SST turbulence model was tested using an optimal grid element size of 0.31M. This model is frequently employed in hypersonic flow analysis due to its precise near-wall modeling, which effectively addresses adverse pressure gradients and minimizes sensitivity to free

stream conditions. Additionally, the K-ω SST model provides a more accurate portrayal of heat transfer on surfaces and walls, making it suitable for minimizing aerothermal temperatures during re-entry [21]. Subsequently, three additional tests were conducted with different turbulence models: K-ε Realizable, K-ε Standard, and LES. Figure 7 shows the variations in pressure coefficients obtained from these models, which are 0.5, 0.8, 0.7, and 6.85 for K-ω SST, K-ε Realizable, K-ε Standard, and LES, respectively.

Additionally, the variation in total temperature of the Reusable Launch Vehicle (RLV) obtained from different turbulence models is presented in Figure 8. The lowest total temperature was observed with the K-ω SST model, approximately 1018 K, whereas the highest total temperature was recorded for the K-ε Realizable model, around 1950 K. The K-ε Standard and LES models yielded total temperatures of approximately 1420 K and 1606 K, respectively. Furthermore, a comparison of the near-wall function visualizations through flow contours of turbulence viscosity for these models is presented in Figure 9. The K-ω SST model demonstrated the most accurate near-wall viscosity, indicating an optimal correlation between grid size and turbulence model for simulating hypersonic flow. In contrast, the LES model only effectively calculated sub-grid viscosity in the rearward region. The K-ε Realizable and K-ε Standard models exhibited nearly similar performance in terms of turbulence viscosity.

These results underscore the importance of selecting an appropriate turbulence model for accurately predicting aerothermal characteristics and ensuring the stability of vehicles during hypersonic re-entry.

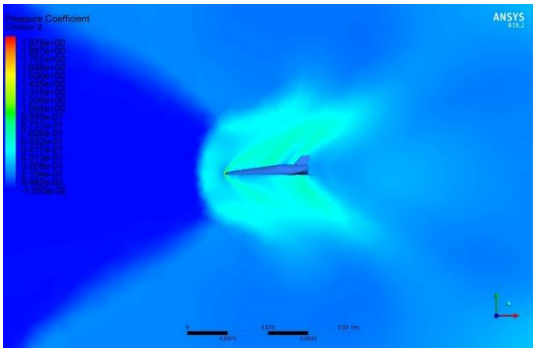

(a)

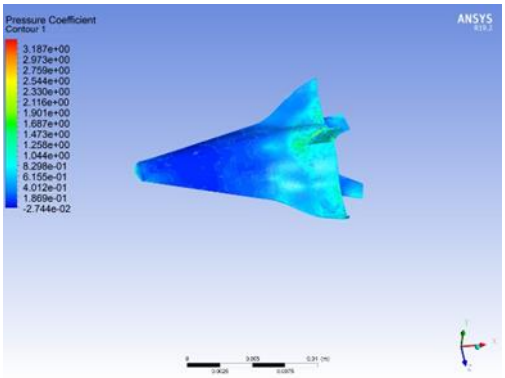

(b)

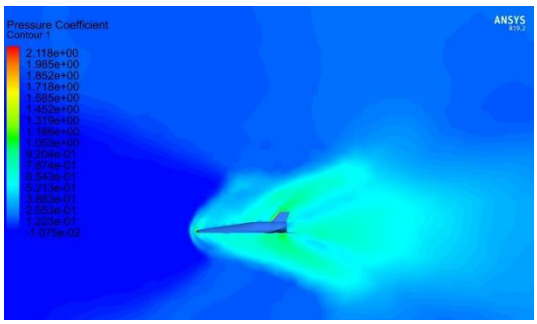

(c)

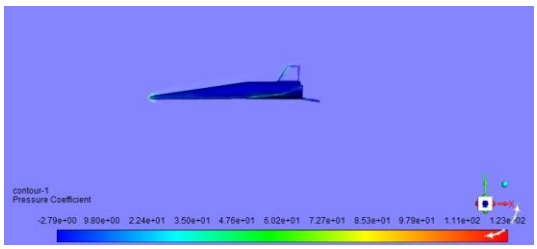

(d)

Figure 7. Variation of Pressure Coefficient for Turbulence Models (a) K-w SST, (b) K-e Realizable, (c) K-e Standard, and (d) LES

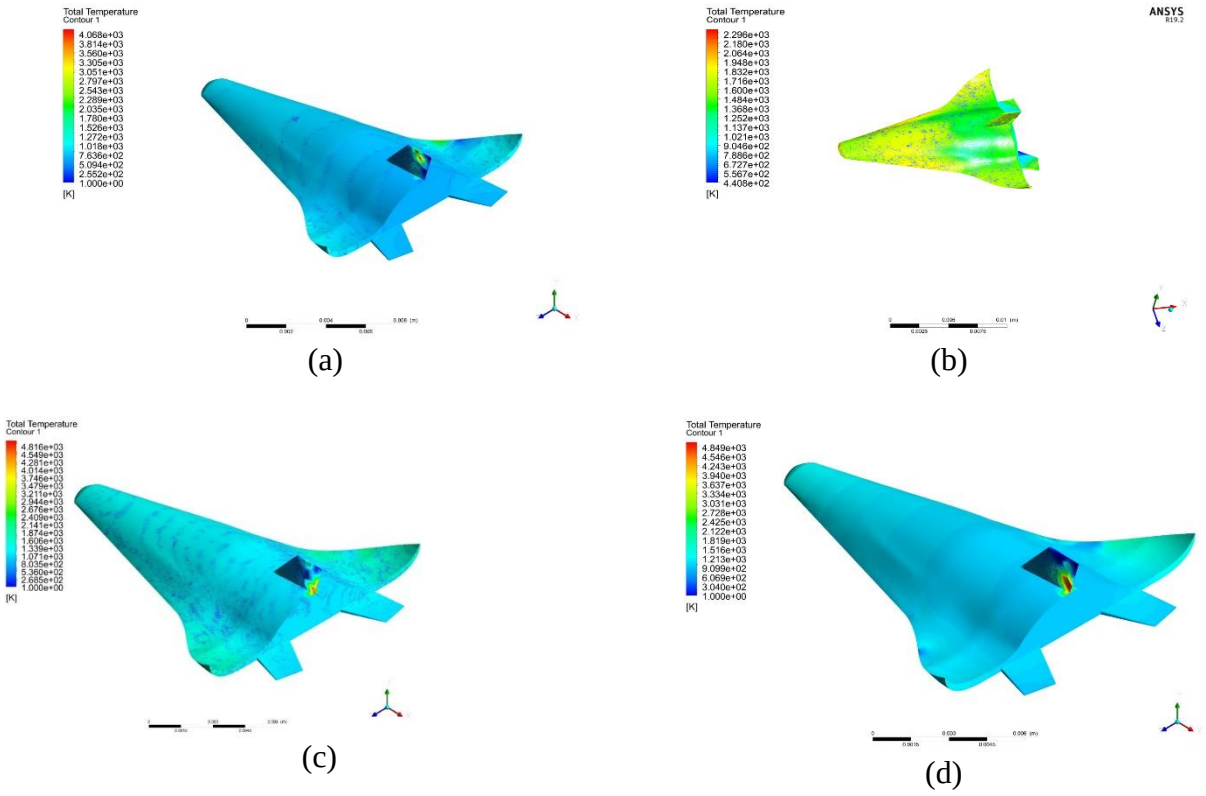

Figure 8. Changes in Total Temperature for Turbulence Models (a) K-w SST, (b) K-e Realizable, (c) K-e Standard, and (d) LES

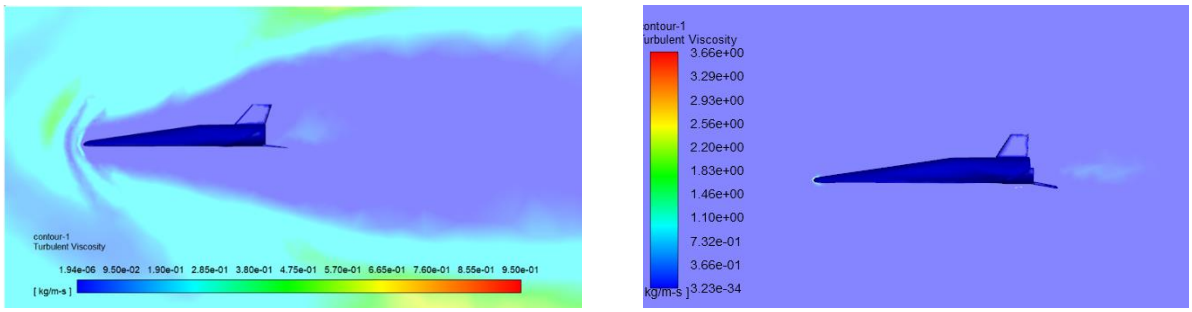

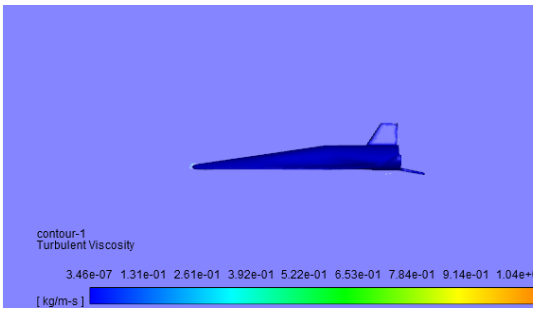

(c) K- ε standard

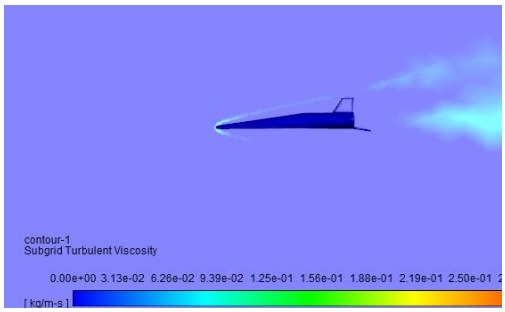

(d) LES

Figure 9. Changes in Turbulence Viscosity for Turbulence Models (a) K-w SST, (b) K-e Realizable, (c) K-e Standard, and (d) LES

Aerodynamic Heating Analysis for Different Mach Cases

Aerodynamic heating analysis is crucial before constructing any real-life hypersonic reusable launch vehicle (RLV) as it ensures the vehicle's thermal protection system can withstand extreme temperatures, safeguarding structural integrity and mission success. In this study, the aerodynamic heating characteristics were also analyzed to predict the better performance of the newly designed RLV at extreme heating conditions at hypersonic speed. The last analysis was carried out utilizing the best grid type along with the well-suited turbulence model K-ω SST where the aerodynamic heating characteristics of the RLV were assessed for different Mach numbers ranging from 5 to 12 and boundary conditions. Initially, the test was conducted using the boundary conditions for Mach number 8.82 as tabulated on

Table 5[29]**.** Following this several other tests were performed to check the better performance of the vehicle for different mach numbers presented in Table 6 below. Figure. 10 shows the variation in lift to drag ratio of the vehicle for altering Mach numbers from 5 to 12 where the larger ratios were obtained from Mach numbers 8.82, and 10.5 which were 2.05, and 3.97 respectively. Besides, for the mach numbers 5 and 7.5 the lift to drag ratio was marked almost similar where the lowest ratio was obtained as 0.029 for Mach 6. Generally, A higher lift-to-drag (L/D) ratio allows for the altitude to be sustained by the vehicle for an extended duration during re-entry, thereby resulting in the mitigation of peak heat flux and overall thermal stress imposed on the thermal protection system (TPS). Therefore, comparing the lift-to-drag ratios for all the mach numbers it can be said that for the mach number 10.5, the vehicle would withstand the re-entry conditions by having comparatively minimal thermal loads and heat flux [30].

Table 5. Free stream conditions

Mach M	Pressure P Pa	Density, kg/m^3 ρ_e	Viscosity μ_e	Velocity, m/s $V\infty$	Temperature, K T_∞
5	1196.22	1.84E-02	1.47E-05	1.70E+03	2.26E+02
6	5529.1	1.23E+00	1.42E-05	2040	216.65
7.5	5529.1	0.0081	1.47E-05	2550	216.65
8	1127.6	0.0081	1.42E-05	2720	252.1
8.82	98635.61	7.07E-04	1.42E-05	2887.3	267
10.5	121000	1.99E-05	1.10E-05	3570	227
12	1.0365	1.99E-05	1.10E-05	4080	180.65

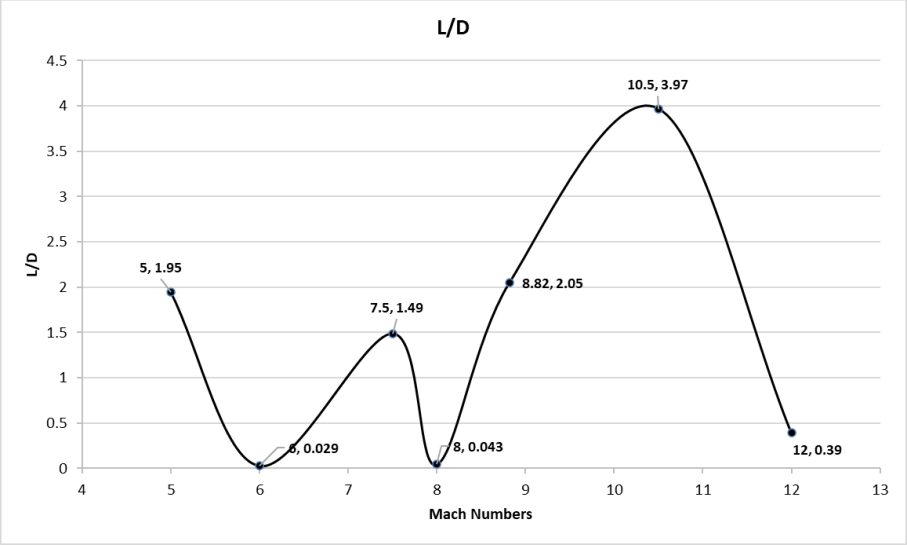

Figure. 10 Lift-to-Drag Ration VS Mach numbers

Moreover, to predict the better aerothermal conditions of the RLV the temperatures obtained from each of the mach cases were compared. By the Figure. 11 it was determined that there is a linear increment in total temperature for mach number 5 to 6 and mach number 10.5 to 12 except the

mach cases 7.5 to 8.82 where the almost similar temperature was predicted for mach 7.5 and 8 which were around 1900. At the nose point, the highest temperature was experienced by the vehicle for every mach cases and gradually it was getting reduced towards the fuselage and tail. However, for mach number 8.82 there was a noticeable reduction in temperature in both nose and body that had a very good agreement with the reference results having only 120 K increments in maximum temperature along with having almost similar results for minimum temperature towards the body [1]. It is obvious that an increase in Mach number or velocities would inevitably cause an increase in the temperature of the RLV body. Nevertheless, the temperature near the wall is reduced by the specific blunt nose on the modeled RLV, which generates a detached shock wave and creates a turbulent wake that lowers the intensity of heat transfer. This design assists in managing and reducing the peak temperatures experienced during high-speed flight [18].

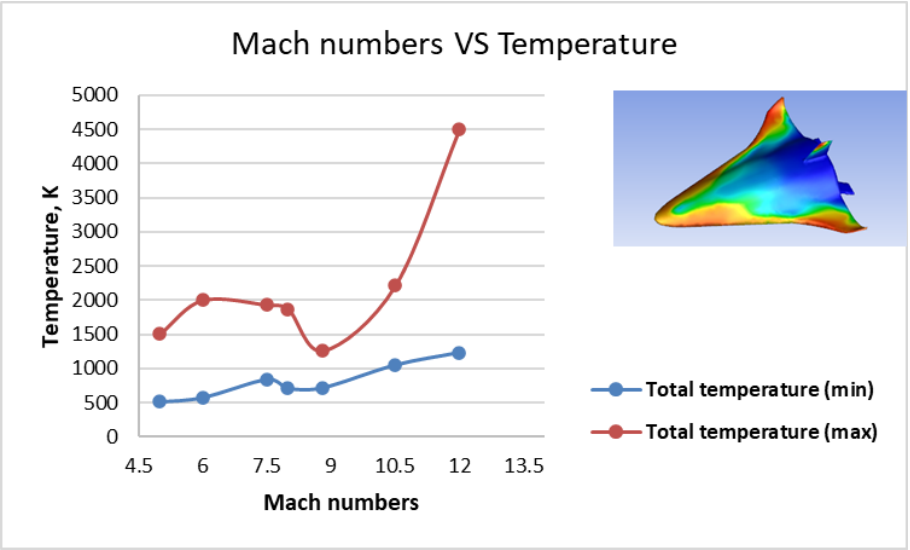

Figure. 11 Mach numbers VS Total Temperature at different positions (a) Nose and (b) Body

A detailed analytical approach was undertaken using the Fay-Riddel equation (6**)** to measure the heat transfer coefficients at the stagnation points of the vehicle [1]. Accurate calculation of these coefficients is crucial for designing the Thermal Protection System (TPS), ensuring that the selected materials and thicknesses can endure the intense heat without failing. Post-calculation, the results were compared with those obtained from the Computational Fluid Dynamics (CFD) study to validate the Mach conditions and the vehicle model during hypersonic re-entry [31].

Table 6 presents the analytically calculated stagnation point heat transfer coefficients for Mach numbers 5 to 12. The results exhibit fluctuations, with higher coefficients observed for Mach numbers 6, 8, and 8.2 (1.38, 1.12, and 0.98 W/m^2-K, respectively). Interestingly, similar coefficients were noted for Mach numbers 5 and 7.5, while the lowest coefficient was recorded for Mach number 12, despite the general trend of increasing heat transfer coefficients with higher Mach numbers. Figure. 12 illustrates the comparison between CFD results and calculated

coefficients. Noticeable discrepancies appear for Mach numbers 8 and 12, whereas minor fluctuations are observed for Mach numbers 5 to 7. The most accurate alignment between CFD and calculated results was found for Mach numbers 10.5 and 8.2, with CFD values of 0.1 and 0.72, and calcuted values of 0.135 and 0.98, respectively. Overall, the least error was found for Mach 10.5, with a 25.9% discrepancy, indicating better accuracy compared to the 26.5% error for Mach 12.

The analysis underscores the challenge of minimizing the stagnation point heat transfer coefficient as velocity increases, which is crucial for reducing thermal loads on re-entry vehicles. The strong shock wave generated by a blunt nose effectively dissipates energy, thereby reducing the heat transferred to the vehicle's stagnation point even if flying at high Mach numbers [32].

Table 6. List of Variables used to calculate stagnation point heat transfer coefficient

Mach	**Density** ρ_e	**Density** (wall) ρ_w	**Viscosity** μ_e	**Viscosity wall** μ_w	**Velocity, m/s** V_∞	**Enthalpy h_s**	**R-eff (ref nose radius, m)**	**Temperature** T_∞	**Velocity gradient DV/Dx**	**SP Heat Transfer Coefficient**
5	1.84E-02	2719(default)	1.47E-05	1.78E-05	1.70E+03	1.82E+06	2.70E-03	2.26E+02	1.34E+05	0.54
6	1.23E+00	2719(default)	1.42E-05	1.78e-05(default)	2040	1822323	0.0027	216.65	3.13E+04	1.38
7.5	0.0081	2719(default)	1.47E-05	1.78e-05(default)	2550	1822323	0.0027	216.65	2.56E+05	0.537
8	0.0081	2719(default)	1.42E-05	1.78e-05(default)	2720	1822323	0.0027	252.1	1.15E+06	1.12
8.82	7.07E-04	2719(default)	1.42E-05	1.78e-05(default)	2887.3	1822323	0.0027	267	6.13E+06	0.98
10.5	1.99E-05	2719(default)	1.10E-05	1.78e-05(default)	3570	1822323	0.0027	227	2.50E+06	0.135
12	1.99E-05	2719(default)	1.10E-05	1.78e-05(default)	4080	1822323	0.0027	180.65	118944.7	0.029

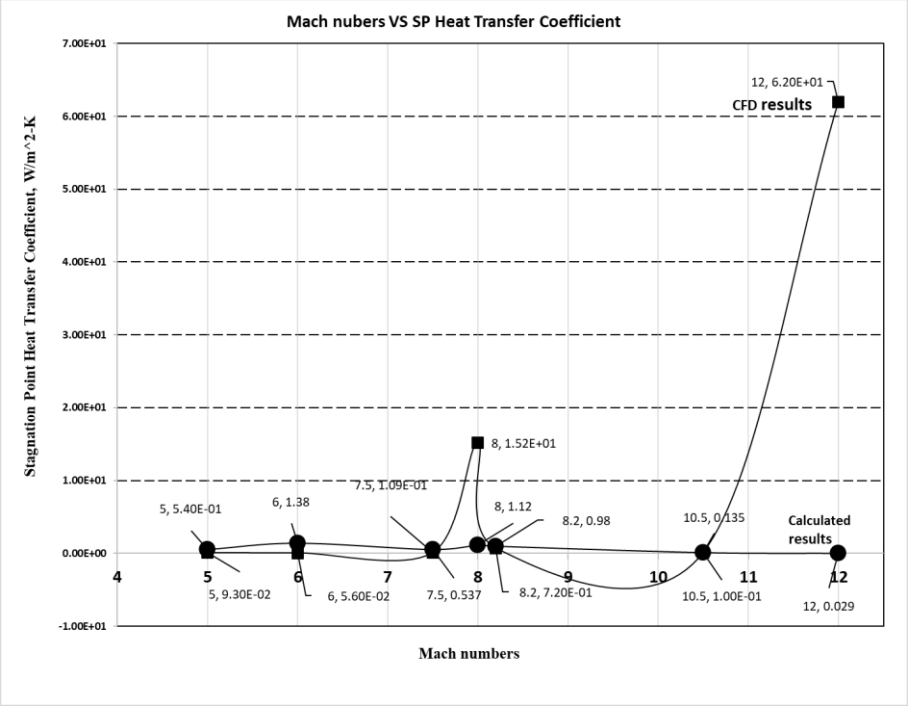

Figure. 12 Comparison between obtained stagnation point heat transfer from CFD and Calculated Stagnation point heat transfer coefficient at different mach cases

To sum up, the combined use of a blunt nose, curved wings, and rear edge flaps significantly enhances the thermal management capabilities of hypersonic re-entry vehicles. The blunt nose reduces the peak heat flux at the stagnation point by dissipating energy through a strong shock wave. Curved wings distribute aerodynamic forces and heat more evenly, while rear edge flaps provide control over the descent trajectory, minimizing sharp changes and localized heating. Together, these design features contribute to a more effective reduction in heat transfer coefficients, ensuring the vehicle's structural integrity and the success of its re-entry mission.

CONCLUSION

This numerical study was carried out to propose a Nobel reusable launched vehicle configuration inspired by HTV and Martin X-33 and analyze its aerodynamic and thermal behaviors during high-speed flight conditions that are very crucial for the implementation of a vehicle’s aerodynamics and thermal management for real-time flight. To predict the aerodynamics of the model in hypersonic conditions and ensure more accuracy the entire research was conducted in three parts- (i) Grid Sensitivity Test, (ii) Turbulence Model Validation Check, and (iii) Aerodynamic Heating Analysis by varying Mach numbers.

The initial stage of this research involved a grid independence study to determine the optimal grid size and quantity for accurately predicting the aerodynamic flow behaviors of a designed Reusable Launch Vehicle (RLV). Using the K-ω SST model and Mach 6, the baseline test with an initial

spacing of 0.09m and Y+ of 1 resulted in 320,738 grid elements and a pressure coefficient (Cp) of 0.98. Additional tests with grid sizes of 70mm, 75mm, 80mm, 85mm, and 95mm showed that grid sizes of 70mm, 80mm, and 85mm produced around 0.31 million elements, while 75mm and 95mm produced approximately 0.42 million elements. The highest Cp of 0.98 was obtained with 0.32 million elements, but a better correlation with reference data was achieved with 0.31 million elements, showing a 6% error. The errors of -31% and -46.9% for grid quantities of 0.32M and 0.42M, respectively, were highlighted by the data obtained from the grid sensitivity validation strengthening the validity of grid quantity of 0.31 over others.

Numerical investigations were conducted utilizing four turbulence models—K-ε Realizable, K-ω SST, K-ε Standard, and LES—to achieve high-fidelity turbulence predictions. The K-ω SST model was initially tested with an optimal grid element size of 0.31M, as it is frequently employed in hypersonic flow analysis due to its precise near-wall modeling capabilities and its effectiveness in addressing adverse pressure gradients. This model also provided a more accurate representation of heat transfer on surfaces and walls, thereby contributing to the minimization of aerothermal temperatures during re-entry. Subsequently, tests were performed with the K-ε Realizable, K-ε Standard, and LES models. The resulting pressure coefficients were recorded as 0.5, 0.8, 0.7, and 6.85, respectively, while the K-ω SST model exhibited the lowest total temperature of approximately 1018 K, in contrast to the K-ε Realizable model, which recorded the highest total temperature of around 2100 K. A comparative analysis of the near-wall function visualizations indicated that the K-ω SST model demonstrated the most accurate near-wall viscosity, whereas the LES model was limited to effectively calculating sub-grid viscosity only in the rearward region.

The aerodynamic heating characteristics of a newly designed Reusable Launch Vehicle (RLV) were analyzed to evaluate its performance under extreme hypersonic conditions. The optimal grid type and the K-ω SST turbulence model were utilized to assess the aerodynamic heating effects across a range of Mach numbers from 5 to 12. Initial tests conducted at a Mach number of 8.82 were validated against reference data, showing a high level of agreement. Subsequent analyses revealed that higher lift-to-drag ratios were achieved at Mach numbers 8.82 and 10.5, with values of 2.05 and 3.97, respectively to contribute to extended altitude sustenance, mitigating peak heat flux and reducing thermal stress on the Thermal Protection System (TPS). Temperature data indicated a general linear increase with Mach numbers, except between Mach 7.5 and 8.82, where temperatures remained relatively consistent. The blunt nose design was observed to reduce peak temperatures by generating a detached shock wave and turbulent wake, thereby decreasing heat transfer intensity. Heat transfer coefficients at stagnation points were calculated using the Fay-Riddel equation, showing variations with the highest coefficients at Mach numbers 6, 8, and 8.2, and the lowest at Mach 12. Comparative analysis of CFD results with analytically calculated coefficients revealed optimal alignment at Mach 10.5, with a discrepancy of 25.9%. This analysis emphasizes the effectiveness of the blunt nose, curved wings, and rear edge flaps in improving thermal management and reducing heat transfer coefficients during hypersonic re-entry, thus enhancing the structural integrity and mission success of the vehicle.

On a whole, it can be said that the newly designed vehicle is likely to achieve optimal performance at Mach 10.5 when the 0.31M grid elements and K-ω SST model are employed for precise assessments. To have more accuracy future research should be directed towards exploring aerodynamic stability under various flight conditions, with an emphasis on utilizing advanced

high-performance computing resources. Detailed insights into aerodynamic and thermal behaviors under extreme conditions are provided by CFD analysis, allowing for accurate predictions and optimization of vehicle performance without the need for costly physical prototypes. Development time and costs are significantly reduced by this approach, enabling safer and more efficient design and testing processes in aerospace engineering.

ACKNOWLEDGEMENTS

I wish to extend my heartfelt thanks to my supervisor, Prof. Srinivas G., Associate Professor, for the opportunity to work on this outstanding project. His invaluable guidance, patience, encouragement, enthusiasm, and extensive knowledge were instrumental in successfully completing my research. This project has significantly enhanced both my research and technical skills. Additionally, I am deeply grateful to my parents and loved ones for their unwavering love, prayers, and constant support, which have motivated me to achieve my goals.

REFERENCES

[1] K. J. Murphy *et al.*, "AIAA Atmospheric Flight Mechanics Conference AIAA 99-4163 X-33 Aerodynamic and Aeroheating Computations for Wind Tunnel and Flight Conditions XÐ33 Aerodynamic and Aeroheating Computations for Wind Tunnel and Flight Conditions," 1999.

[2] P. C. Chen *et al.*, "Aerothermodynamic Optimization of Hypersonic Vehicle TPS Design by a POD/RSM-Based Approach," 2006.

[3] D. Bhalla, G. Vidya, and M. T. Nair, "Aerothermal Characterisation of a Typical Re-entry Module in Hypersonic Flow Regime," in *Lecture Notes in Mechanical Engineering*, Springer Science and Business Media Deutschland GmbH, 2023, pp. 541–546. doi: 10.1007/978-981-19-6270-7_90.

[4] S. H. Park, D. Neeb, G. Plyushchev, P. Leyland, and A. Gülhan, "A study on heat flux predictions for re-entry flight analysis," *Acta Astronaut*, vol. 187, pp. 271–280, Oct. 2021, doi: 10.1016/j.actaastro.2021.06.025.

[5] F. Battista, G. C. Rufolo, and M. Di Clemente, "Aerothermal environment definition for a reusable experimental re-entry vehicle wing," in *Collection of Technical Papers - 39th AIAA Thermophysics Conference*, 2007, pp. 378–397. doi: 10.2514/6.2007-4048.

[6] S. Di Giorgio, D. Quagliarella, G. Pezzella, and S. Pirozzoli, "An aerothermodynamic design optimization framework for hypersonic vehicles."

[7] S. G. Sheffer, G. S. Dulikravich, S. G. Sheffer, and G. S. Dulikravich, "AIAA 93-0039 Constrained Optimization of Three-Dimensional Hypersonic Vehicle Configurations

CONSTRAINED OPTIMIZATION OF THREE-DIMENSIONAL HYPERSONIC VEHICLE CONFIGURATIONS."

[8] K. G. Bowcutt, "Multidisciplinary optimization of airbreathing hypersonic vehicles," *J Propuls Power*, vol. 17, no. 6, pp. 1184–1190, 2001, doi: 10.2514/2.5893.

[9] M. A. Lobbia, "Rapid supersonic/hypersonic aerodynamics analysis model for arbitrary geometries," *J Spacecr Rockets*, vol. 54, no. 1, pp. 315–322, 2017, doi: 10.2514/1.A33514.

[10] J. J. Mcnamara and P. P. Friedmann, "Aeroelastic and Aerothermoelastic Analysis of Hypersonic Vehicles: Current Status and Future Trends," 2007.

[11] V. V. Kuzenov, S. V. Ryzhkov, and A. Y. Varaksin, "Calculation of Heat Transfer and Drag Coefficients for Aircraft Geometric Models," *Applied Sciences (Switzerland)*, vol. 12, no. 21, Nov. 2022, doi: 10.3390/app122111011.

[12] G. Pezzella and A. Viviani, "Aerodynamic performance analysis of a winged re-entry vehicle from hypersonic down to subsonic speed," *Aerosp Sci Technol*, vol. 52, pp. 129–143, May 2016, doi: 10.1016/j.ast.2016.02.030.

[13] "Journal of Mines, Metals and Fuels", doi: 10.18311/jmmf/2023.

[14] Pradeep Kumar Sulur Loganathan, "Design and CFD Analysis on the Reduction of Thermal Effect in Re-entry Vehicle by Using Retractable Aerospike," *Hypersonic and Supersonic Flight - Advances in Aerodynamics, Materials, and Vehicle Design*, Nov. 2022.

[15] A. Murray, "AEROHEATING ANALYSIS FOR PLANETARY RE-ENTRY VEHICLES."

[16] A. and N. S. R. G. Gopala Krishnan, "DRAG REDUCTION FOR HYPERSONIC RE-ENTRY VEHICLES ," *International Journal of Mechanical Engineering and Technology (IJMET)* , vol. 08, no. 10, Oct. 2017.

[17] T. N. A. O. and K. F. 17. Tomoaki TATSUKAWA, "Aerodynamic design exploration for reusable launch vehicle using genetic algorithm with navier stokes solver," in *Proceedings of the ASME Design Engineering Technical Conference*, 2011, pp. 213–223.

[18] J. D. Anderson Jr., *Hypersonic and High-Temperature Gas Dynamics, Second Edition*. 2006. doi: 10.2514/4.861956.

[19] V. S. Rao, V. Viti, and J. Abanto, "Cfd simulations of super/hypersonic missiles: Validation, sensitivity analysis, and improved design," in *AIAA Scitech 2020 Forum*, American Institute of Aeronautics and Astronautics Inc, AIAA, 2020. doi: 10.2514/6.2020-2123.

[20] P. Papadopoulos, E. Venkatapathy, D. Prabhu, M. P. Loomis, and D. Olynick, “Current grid-generation strategies and future requirements in hypersonic vehicle design, analysis and testing.” [Online]. Available: www.elsevier.nl/locate/apm

[21] L. Könözsy, “The k-ω Shear-Stress Transport (SST) Turbulence Model,” *A New Hypothesis on the Anisotropic Reynolds Stress Tensor for Turbulent Flows, Fluid Mechanics and Its Applications*, 2019.

[22] F. Rahman and G. Srinivas, “Aerodynamic Performance Enhancement of Electromagnetic Gun Projectile Using Numerical Techniques,” *Journal of Advanced Research in Fluid Mechanics and Thermal Sciences*, vol. 80, no. 2, pp. 136–152, 2021, doi: 10.37934/arfmts.80.2.136152.

[23] S. Younoussi and A. Ettaouil, “Calibration method of the k-ω SST turbulence model for wind turbine performance prediction near stall condition,” *Heliyon*, vol. 10, no. 1, Jan. 2024, doi: 10.1016/j.heliyon.2024.e24048.

[24] A. Kulinich, “Computation of Approximate Stagnation Point Heat Flux in Hypersonic Flow at Any Mach Number and Altitude: A Python-Based Numerical Approach,” 2023.

[25] M. R. Malik, “Numerical methods for hypersonic boundary layer stability,” *J Comput Phys*, vol. 86, no. 2, pp. 376–413, 1990, doi: 10.1016/0021-9991(90)90106-B.

[26] R. D. Quinn and L. Gong, “NASA Technical Memorand_ 4222 Real-Time Aerodynamic Heating and Surface Temperature Calculations for Hypersonic Flight Simulation.”

[27] J. Cheng, R. Chen, R. Qiu, W. Sun, and Y. You, “Aerothermodynamic study of Two-Stage-To-Orbit system composed of wide-speed-range vehicle and rocket,” *Acta Astronaut*, vol. 183, pp. 330–345, Jun. 2021, doi: 10.1016/j.actaastro.2020.11.034.

[28] Y. Zhao, C. Yan, X. Wang, H. Liu, and W. Zhang, “Uncertainty and sensitivity analysis of SST turbulence model on hypersonic flow heat transfer,” *Int J Heat Mass Transf*, vol. 136, pp. 808–820, Jun. 2019, doi: 10.1016/j.ijheatmasstransfer.2019.03.012.

[29] K. J. Murphy *et al.*, “AIAA Atmospheric Flight Mechanics Conference AIAA 99-4163 X-33 Aerodynamic and Aeroheating Computations for Wind Tunnel and Flight Conditions XÐ33 Aerodynamic and Aeroheating Computations for Wind Tunnel and Flight Conditions,” 1999.

[30] “High Lift-over-Drag Earth Re-entry High Lift-over-Drag Earth Re-entry,” 2009.

[31] A. Kulinich, “Computation of Approximate Stagnation Point Heat Flux in Hypersonic Flow at Any Mach Number and Altitude: A Python-Based Numerical Approach,” 2023.

[32] S. H. Park, D. Neeb, G. Plyushchev, P. Leyland, and A. Gülhan, “A study on heat flux predictions for re-entry flight analysis,” *Acta Astronaut*, vol. 187, pp. 271–280, Oct. 2021, doi: 10.1016/j.actaastro.2021.06.025.